

# Dissociation of Recombinant Prion Protein Fibrils into Short Protofilaments: Implications for the Endocytic Pathway and Involvement of the N-Terminal Domain

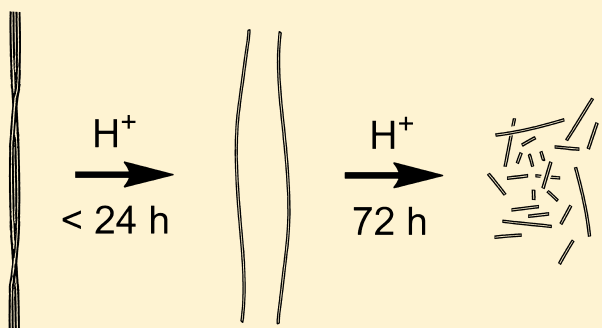
Xu Qi,<sup>†</sup> Roger A. Moore,<sup>‡</sup> and Michele A. McGuire<sup>\*,†</sup>

<sup>†</sup>Center for Biomolecular Structure and Dynamics and Division of Biological Sciences, 204 CHCB, The University of Montana, Missoula, Montana 59812, United States

<sup>‡</sup>Rocky Mountain Laboratories/Laboratory of Persistent Viral Diseases, National Institute of Allergy and Infectious Diseases, National Institutes of Health, 903 South 4th Street, Hamilton, Montana 59840, United States

## S Supporting Information

**ABSTRACT:** Fibril dissociation is necessary for efficient conversion of normal prion protein to its misfolded state and continued propagation into amyloid. Recent studies have revealed that conversion occurs along the endocytic pathway. To improve our understanding of the dissociation process, we have investigated the effect of low pH on the stability of recombinant prion fibrils. We show that under conditions that mimic the endocytic environment, amyloid fibrils made from full-length prion protein dissociate both laterally and axially to form protofilaments. Approximately 5% of the protofilaments are short enough to be considered soluble and contain ~100–300 monomers per structure; these also retain the biophysical characteristics of the filaments. We propose that protonation of His residues and charge repulsion in the N-terminal domain trigger fibril dissociation. Our data suggest that lysosomes and late endosomes are competent milieus for propagating the misfolded state not only by destabilizing the normal prion protein but also by accelerating the dissociation of fibrils into smaller structures that may act as seeds.



The normal cellular form of prion protein (PrP<sup>C</sup>) is a monomeric glycoprotein that is tethered to the plasma membrane via its glycosylphosphatidylinositol anchor.<sup>1</sup> It is expressed in all mammals and avian species with a high level of expression in the central nervous system, especially on the presynaptic membrane.<sup>2,3</sup> Natively folded PrP<sup>C</sup> is characterized by a large unstructured N-terminal domain (residues 23–89), a hydrophobic region within residues 90–124, and a well-ordered C-terminal domain (residues 125–228) composed of three  $\alpha$ -helices and two short antiparallel  $\beta$ -strands. A short flexible segment of four amino acids at the C-terminus links to the GPI anchor,<sup>4–7</sup> and there are two sites of glycosylation located within the structured domain.

Conversion from PrP<sup>C</sup> to its misfolded conformer is associated with a group of neurodegenerative diseases known as prion diseases.<sup>8,9</sup> This conformer is called PrP<sup>Sc</sup>, where Sc denotes scrapie, the ovine disease. Unlike PrP<sup>C</sup>, PrP<sup>Sc</sup> is an insoluble, partially proteinase K-resistant amyloid aggregate.<sup>7</sup> A growing body of evidence suggests that the neurotoxic entity responsible for prion disease is a soluble prefibrillar intermediate or an off-pathway product generated intra-neuronally during PrP<sup>C</sup> to PrP<sup>Sc</sup> conversion.<sup>10–14</sup> However, our understanding is limited because of the lack of a precise physical definition for these soluble intermediates.

PrP<sup>C</sup> to PrP<sup>Sc</sup> conversion occurs through the direct interaction between PrP<sup>C</sup> and PrP<sup>Sc</sup>, in which the PrP<sup>Sc</sup> acts as a conformational template, causing PrP<sup>C</sup> to misfold and extend the amyloid aggregate.<sup>13,15</sup> For efficient propagation of the aggregate, PrP<sup>Sc</sup> must dissociate into smaller nuclei that can seed additional conversions in a process known as secondary nucleation.<sup>15–17</sup> Thus, the rate of fibril dissociation contributes significantly to the overall rate of propagation.<sup>18,19</sup>

Studies of mammalian PrP suggest that the conversion of PrP<sup>C</sup> to PrP<sup>Sc</sup> takes place both on the plasma membrane and along the endocytic pathway.<sup>14,20–23</sup> The majority of PrP<sup>Sc</sup> has been shown to accumulate in the lysosomes of infected cells.<sup>24</sup> Interestingly, *Atg5*<sup>−/−</sup> fibroblasts, which lack the ability to execute autophagy and then transport PrP<sup>Sc</sup> aggregates into lysosomes, show significantly increased resistance to prion infection.<sup>25</sup> Together, these results indicate that there must be a mechanism within the endocytic pathway for the dissociation of the mature PrP<sup>Sc</sup> into seeds and thus the continuation of its efficient propagation.<sup>13</sup> One potential environmental contributor to dissociation is the acidic pH of lysosomes.<sup>26</sup>

Received: February 14, 2012

Revised: May 11, 2012

Published: May 16, 2012



We have observed that the solution circular dichroism (CD) spectrum for amyloid fibrils generated from full-length recombinant hamster prion protein (rPrP23–232) can be measured only at acidic pH. As large fibrils merely scatter the CD light, we postulated that dissociation of some fibrils was occurring under acidic conditions. We therefore investigated the behavior of recombinant PrP fibrils under mildly acidic conditions that mimic the endocytic environment. We demonstrate that full-length fibrils dissociate both laterally and axially to form shorter oligomeric structures we term protofilaments; ~5% of these are soluble and contain ~100–300 monomers. The protofilaments retain the characteristic intermolecular  $\beta$ -sheet structure of the mature fibrils. We propose that protonation of histidine residues in the N-terminal region of PrP is involved in fibril dissociation, suggesting that this region, which is intrinsically disordered in the normal cellular PrP<sup>C</sup>, might take on structure when amyloid fibrils are formed. Our results provide evidence of the molecular events that may occur during prion propagation in vivo.

## ■ EXPERIMENTAL PROCEDURES

The genes encoding residues 23–232 or 90–232 of golden Syrian hamster prion protein were amplified by polymerase chain reaction from plasmid pHaPrP<sup>27</sup> and inserted into pET24, and the recombinant protein was expressed in BL21(DE3)-Rosetta cells (Novagen). The results were confirmed by DNA sequencing (Murdock Sequencing Facility, The University of Montana).

Recombinant hamster prion proteins (rPrP23–232 or rPrP90–232) were expressed and purified using minor modifications of published protocols.<sup>27,28</sup> The purity of rPrP was confirmed by sodium dodecyl sulfate–polyacrylamide gel electrophoresis (SDS–PAGE) on a PhastSystem (GE Healthcare, Inc.). Stocks of purified protein were stored in 6 M GdnHCl and 0.1 M phosphate (pH 8.0). The protein concentration was determined spectrophotometrically in 6 M GdnHCl using an  $\epsilon_{280}$  of 61025 M<sup>−1</sup> cm<sup>−1</sup> for rPrP23–232 and 24345 M<sup>−1</sup> cm<sup>−1</sup> for rPrP90–232, as calculated using ProtParam on the ExPASy web server.<sup>29</sup>

The  $\alpha$ -helical, PK sensitive monomeric form of rPrP ( $\alpha$ -monomer), which is structurally similar to PrP<sup>C</sup> but lacks the GPI anchor and glycosylation,<sup>30</sup> was formed by extensively dialyzing the stock solution against 20 mM acetate (pH 4.5). We also prepared a previously characterized octameric conformer that is highly enriched in  $\beta$ -sheet structure, which is termed the  $\beta$ -oligomer.<sup>28,31</sup> The secondary structures of the  $\alpha$ -monomer and  $\beta$ -oligomer were confirmed using CD.

The initial PK-resistant amyloid-like fibrils were generated by 3-fold dilution of the  $\alpha$ -monomer into denaturant fibrillation buffer to give a final concentration of ~1 mg/mL rPrP in 15 mM phosphate, 0.5 M guanidine (GdnHCl), and 1.2 M urea (pH 6.5).<sup>32–34</sup> Samples were incubated at 37 °C under continuous orbital shaking at 600 rpm in 1.5 mL siliconized Eppendorf tubes, and fibrils were collected by centrifugation at 15000g for 10 min. The amyloid nature and morphological characteristics of the fibrils were confirmed by ThT fluorescence assay<sup>35</sup> and transmission electron microscopy (TEM), respectively.

To test the effects of low pH on the stability of rPrP fibrils, ~300  $\mu$ M rPrP fibrils were incubated in 20 mM acetate (pH 4.5) at 37 °C for 3 days, with continuous rotation at 8 rpm to prevent fibrils from settling. Ultracentrifugation was conducted in a TLA-55 rotor at 120000g for 2 h.

Prion conformers were isolated, analyzed, and sized by asymmetric flow field flow fractionation (AF4) on an AF2000 instrument (PostNova, Inc.), equipped with in-line UV–vis and seven-angle light scattering detectors.<sup>28,36</sup> Samples were loaded in one 20–30  $\mu$ L injection, focused for 4 min with a crossflow of 3.5 mL/min on a regenerated cellulose membrane (5 kDa MWCO), and then eluted at a channel flow rate of 1.5 mL/min and a crossflow of 2.5 mL/min for 30 min. The crossflow was linearly decreased to 0.1 mL/min over 10 min and then held constant for 30 min.<sup>37,38</sup> The molar mass and radius of gyration ( $R_g$ ) of the protofilament peak were determined from the light scatter using PostNova software<sup>39</sup> and evaluated using the Berry method.<sup>40,41</sup>

The  $R_g$  of the soluble protofilaments was also estimated from transmission electron microscopy (TEM) images using the standard formula for the moment of inertia of a rigid, solid cylinder and the mean width and length.<sup>42</sup> TEM was conducted at the Electron Microscopy Facility of The University of Montana. A 5  $\mu$ L aliquot of sample (20–50  $\mu$ M) was cast on a Formvar-coated copper grid and allowed to adsorb for 3–30 min in a constant-humidity chamber. The grid was then rinsed with distilled water and stained with 2% (w/v) uranyl acetate for 30 s before being briefly washed again with water. Varying the staining time did not change the results. After being air-dried, the sample was viewed using a Hitachi H-7100 instrument at 75 kV at standard magnifications of 20000 $\times$  and 100000 $\times$ .<sup>35</sup> Fibril dimensions were determined using ImageJ (National Institutes of Health, Bethesda, MD). Between 30 and 450 individual structures were measured per image; widths and lengths are reported as means  $\pm$  the standard deviation (SD), and average lengths are reported as the geometric mean.

CD spectra were recorded on a Jasco 810 spectrophotometer equipped with a Peltier temperature controller. Parameters were as follows: 1 mg/mL rPrP; path, 0.01 cm; response time, 4 s; five spectra averaged.<sup>43</sup> Protein secondary structure analysis was performed using the DICHROWEB server and CDSSTR<sup>44,45</sup> with Reference Data Set 3.

FT-IR spectroscopy was performed using a Thermo Nicolet NEXUS 670 spectrometer with continuous nitrogen purge. Samples were exchanged into D<sub>2</sub>O buffer and analyzed in a demountable liquid cell fitted with two CaF<sub>2</sub> windows separated by a 50  $\mu$ m Teflon spacer. Spectra were obtained from 128 cumulative scans from 1400 to 2000 cm<sup>−1</sup> at 2 cm<sup>−1</sup> resolution and corrected by scaled subtraction of a water vapor spectrum until the region from 1900 to 1750 cm<sup>−1</sup> no longer showed a negative lobe.<sup>46,47</sup>

Samples for PK digestion were adjusted to 2 mg/mL in either 15 mM phosphate (pH 6.5) or 20 mM acetate (pH 4.5). PK digestion was performed for 2 h at 37 °C at a PK:rPrP ratio of 1:10. Digestion products were separated by SDS–PAGE on a PhastSystem using high-density gels (GE Healthcare Life Sciences) and analyzed versus the migration of peptide standards (MW-SDS-17S, Sigma). For MALDI-ToF/ToF analysis, in-gel tryptic digestion was also performed.<sup>48</sup> Data were processed using mMass.<sup>49</sup>

The kinetics of the formation of fibril from the  $\alpha$ -monomer was monitored under de novo (unseeded) and seeded conditions, where the seeds were soluble protofilaments purified as described in the next paragraph. No denaturants were used. Conversion was conducted at 37 °C in a 96-well plate (Corning product no. 3651) with a total reaction volume of 0.2 mL/well containing 50  $\mu$ M  $\alpha$ -monomer in 20 mM

acetate with or without 0.1 M NaCl (pH 4.5) and 10  $\mu$ M ThT; at this concentration, ThT has a negligible effect on the kinetics of fibril formation.<sup>50</sup> Plates were sealed and incubated at 37 °C in the SpectraMax M2<sup>e</sup> Microplate Reader (Molecular Devices). The fluorescence emission intensity at 488 nm was recorded hourly ( $\lambda_{\text{ex}}$  445 nm) after the plate had been briefly shaken.

## RESULTS

### Acidic Conditions Induce Protofilament Formation.

Negative stain TEM images revealed that fibrils formed under partially denaturing conditions from either N-terminally truncated rPrP90–232 or full-length rPrP23–232 consisted of long, unbranched structures. These were typically well over 1000 nm in length, with widths of  $27 \pm 2$  and  $27 \pm 3$  nm (mean  $\pm$  SD) (Figure 1), respectively. Both fibrils displayed twists, with periodicities of  $\sim 180$  nm for rPrP90–232 and  $\sim 250$ – $360$  nm for rPrP23–232. This suggests that the fibrils are composed of at least two thinner strands, as has previously been described,<sup>32,51</sup> and we refer to them as protofilaments. The amyloid nature of these fibrils was further confirmed by high ThT fluorescence (Figure S1 of the Supporting Information).

To determine whether the acidic environment of endosomes might encourage fibril dissociation, rPrP90–232 and rPrP23–232 fibrils were resuspended in pH 4.5 buffer for 3 days. TEM showed that the morphology of the rPrP90–232 fibrils was unaffected by the decrease in pH; no changes in twist, width, or length were noted (Figure 1A–D). In contrast, the rPrP23–232 sample was dramatically different. TEM revealed that at low pH the fibrils were changed into a population of structures of various lengths that were devoid of twist (Figure 1E–H). We then used ultracentrifugation to isolate the smallest of these structures, which were recovered from the supernatant and deemed soluble according to the standards of Hjelmeland and Chrambach.<sup>52</sup> Approximately 5% of the original rPrP23–232 fibrils was present in the supernatant (Figure 1I). The lengths of these soluble structures ranged from 20 to 150 nm (mean of 65 nm). We also noted an approximate 50% decrease in width [ $15 \pm 2$  nm (supernatant) and  $14 \pm 2$  nm (pellet)] and a lack of twist for both the soluble and insoluble fractions (Figure 1I, J).

**Composition of the Protofilament Amyloid Core.** To compare the composition of the amyloid cores of the protofilaments with those of their parent fibrils, we performed proteinase K (PK) digestion. Full-length PrP fibrils were digested at pH 6.5 and also after the fibrils had been resuspended in pH 4.5 buffer. In the pH 4.5 experiments, PK digestion was performed immediately after the change in pH and again 72 h later. TEM imaging indicated that at 72 h, the sample has mostly dissociated into protofilaments of varying lengths. This preincubated sample was further processed by centrifugation to remove the majority of the insoluble protofilaments prior to PK digestion.

The results were then analyzed by SDS–PAGE (Figure 2, top). At pH 6.5 (lane 1), the most intense PK-resistant band is at  $\sim 5.5$  kDa, although bands at 5 and 7 kDa are also visible. Lane 2 shows the results of the sample digested immediately after the pH was lowered to 4.5. A triplet of bands at 7, 9, and 12 kDa is detected. This shift of the PK-resistant PrP bands with pH is attributed to the pH dependence of PK specificity.<sup>53</sup> The same triplet was also present in the preincubated sample (lane 3), although the band intensities were slightly different.

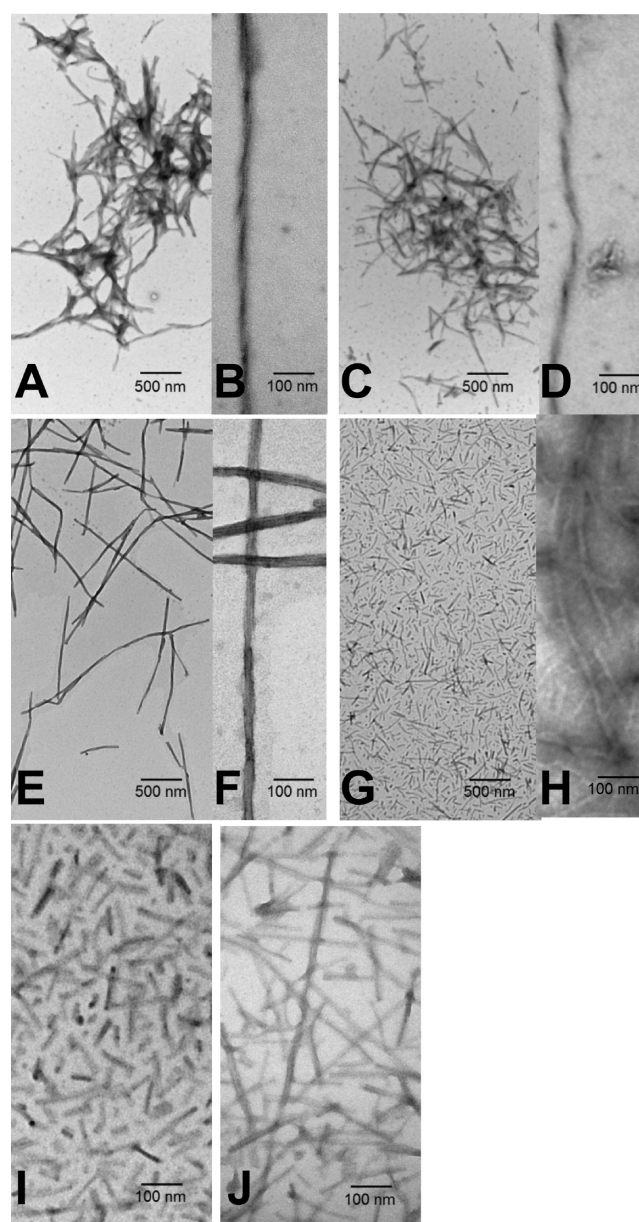


**Figure 1.** TEM images of rPrP23–232 and rPrP90–232 fibrils showing pH-triggered dissociation of full-length fibrils. Images were taken at 20000 $\times$  (scale bar of 500 nm) or 100000 $\times$  magnification (scale bar of 100 nm): (top) truncated rPrP90–232 fibrils at pH 6.5 (A and B) and after being stored for 3 days at pH 4.5 (C and D), (middle) full-length rPrP23–232 fibrils at pH 6.5 (E and F) and after being stored for 3 days at pH 4.5 (G and H). The sample in panels G and H was ultracentrifuged to separate the soluble portion (I) from the insoluble portion (J).

For control purposes, PK digestion of truncated rPrP90–232 fibrils was also performed (Figure 2, bottom). Conditions were identical to those used for full-length PrP except that the centrifugation step was omitted from the sample that was preincubated, because no protein could be found in the supernatant. As expected, the 72 h preincubation had no effect on the PK resistance, as the truncated fibrils do not dissociate at low pH. There were slight variations in the band intensities, but overall, the PK resistance of truncated fibrils was similar to that of full-length PrP.



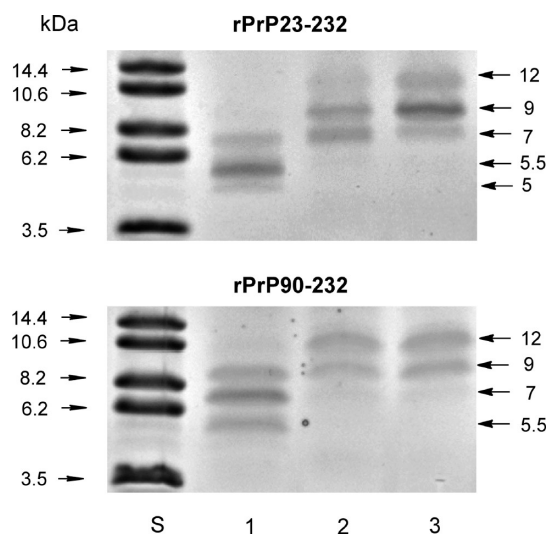


**Figure 2.** SDS–PAGE analysis of the PK-resistant regions of rPrP fibrils and protofilaments: lane S, molecular mass standards; lane 1, pH 6.5; lane 2, pH 4.5; lane 3, samples preincubated at pH 4.5 for 72 h prior to PK digestion. For samples in lane 3, the full-length sample was centrifuged prior to digestion but the truncated sample was not.

For each gel lane in Figure 2, the peptide bands were excised, digested with trypsin, and analyzed by mass spectrometry to map the composition of each fragment (Table S1 and Figure S2 of the Supporting Information). No peptides from residues 23–137 were detected in any PK-resistant fragment. This confirmed that protofilament formation did not involve refolding of all or part of the N-terminal domain into a PK-resistant  $\beta$ -sheet structure. The data in Table S1 of the Supporting Information show that the 12, 9, and 7 kDa peptide fragments begin at residues 137, 149, and 157, respectively. There was little difference in the MS data collected for identical masses derived from different gel lanes.

The identity of the 7 kDa peptide (approximately residues 157–220) is consistent with the amyloid core detected by hydrogen–deuterium exchange mass spectrometry<sup>54</sup> and site-directed spin labeling electron paramagnetic resonance spectroscopy<sup>55</sup> for human rPrP90–232. We attribute the presence of larger peptide fragments in these samples to the inability of PK to fully access non-amyloid regions of PrP.<sup>54</sup> PK-resistant, nonspecific aggregates have been shown to form after the N-terminal domain of amyloid PrP has been cleaved and/or partially digested.<sup>32</sup> It is believed that the exposure of hydrophobic residues causes nonspecific aggregation that impedes PK digestion. Therefore, the presence of larger PK-resistant peptides noted in Figure 2 does not mean that the amyloid core of the protofilaments has extended beyond the 7 kDa  $\beta$ -sheet core identified for recombinant PrP fibrils by other techniques.<sup>55</sup>

Overall, it appears that fibrils and protofilaments possess similar global architectures in their amyloid core regions; there is no evidence that protofilament formation involves reorganization of the N-terminal domain into an amyloid state.

**Purification and Size Determination of Soluble Protofilaments.** We used asymmetric flow field flow fractionation (AF4) and multiangle light scattering to further purify and analyze the soluble protofilaments of rPrP23–232 that were isolated by ultracentrifugation (Figure 3A). Small amounts of  $\alpha$ -monomer and  $\beta$ -oligomer were present in the supernatant, eluting at 6.8 and 20.9 min, respectively. Their

identities were confirmed by circular dichroism (CD)<sup>28,31</sup> (shown in Figure 3B). The majority of the sample eluted under low crossflow at 42.6 min. The molar mass elugram (Figure S3 of the Supporting Information) revealed this peak had significant polydispersity with the centroid at 5.8 MDa, which is equivalent to  $\sim 250$  monomeric subunits. The radius of gyration ( $R_g$ ) for the species that eluted at the centroid is 29.5 nm. This is consistent with the  $R_g$  value of 27 nm that we estimated from the TEM images. This value was calculated using the average radius of 7 nm and a mean particle length of 65 nm (Figure 11) and treating the protofilaments as rigid cylinders. This confirms that the soluble protofilaments observed by TEM are the main constituent purified by AF4 from the supernatant.

As expected, no peaks were observed in the supernatant of low-pH-treated rPrP90–232 fibrils (Figure 3A). Re-injection of the 42.6 min peak after storage for an additional 3 days showed no significant changes. SDS–PAGE analysis confirmed that the purified protofilaments contain full-length rPrP; no degradation products were observed (data not shown). These results demonstrate that the soluble protofilaments are quite stable under acidic conditions. Axial dissociation of the long, insoluble protofilaments to form short, soluble structures reached a steady state maximum after incubation for  $\sim 2$  days at pH 4.5 (Figure 3C).

**pH Dependence of Protofilament Formation.** To confirm the pH-dependent nature of dissociation, we assessed the stability of rPrP23–232 fibrils after incubation at pH 6.5, 5.5, and 4.5 for 3 days. AF4 analysis (Figure 3D) showed that soluble protofilaments are also formed at pH 5.5, although the centroid of the protofilament peak shifted to a slightly higher apparent molecular mass (43.7 min, 8.5 MDa,  $\sim 370$  monomers) compared with the results obtained at pH 4.5. No short protofilaments were formed at pH 6.5. These data confirm that the fibril dissociation and size distribution of the products are pH-dependent, and that rPrP23–232 fibrils are stable under neutral conditions. The amyloid nature of the soluble protofilaments was confirmed by their resistance to thermal denaturation and the ThT fluorescence assay (Figure S1 of the Supporting Information). The dissociation of mature fibrils into protofilaments occurred in the presence and absence of 0.1 M NaCl, although the dissociation into short protofilaments took longer when salt was included (see Figure S4 of the Supporting Information).

**Circular Dichroism Spectroscopy.** The CD spectrum of the soluble protofilament fraction (42.6 min peak) is shown in Figure 3B, along with that of  $\alpha$ -monomer and  $\beta$ -oligomer. The protofilament signal is markedly different from those of both the  $\alpha$ -monomer and the  $\beta$ -oligomer. A single negative peak centered at 216 nm was associated with a rather large MRE value ( $-12000 \text{ deg cm}^2 \text{ dmol}^{-1} \text{ residue}^{-1}$ ). Secondary structure analyses indicate that the soluble protofilaments have considerably less  $\alpha$ -helix and more  $\beta$ -sheet in comparison with the  $\alpha$ -monomer (Table 1).<sup>44,45</sup> Although the overall shapes and MRE values of the protofilaments and the  $\beta$ -oligomer are quite different, the predicted secondary structure content is surprisingly similar. However, CD spectroscopy often misestimates the  $\beta$ -sheet content because of the significant overlap of the  $\beta$ -sheet absorption band with that from  $\alpha$ -helices. We could not obtain a solution CD spectrum of fibrils at neutral pH for direct comparison with the protofilaments, probably because they scatter too much light. The similar solution CD spectrum of fibrils has been previously

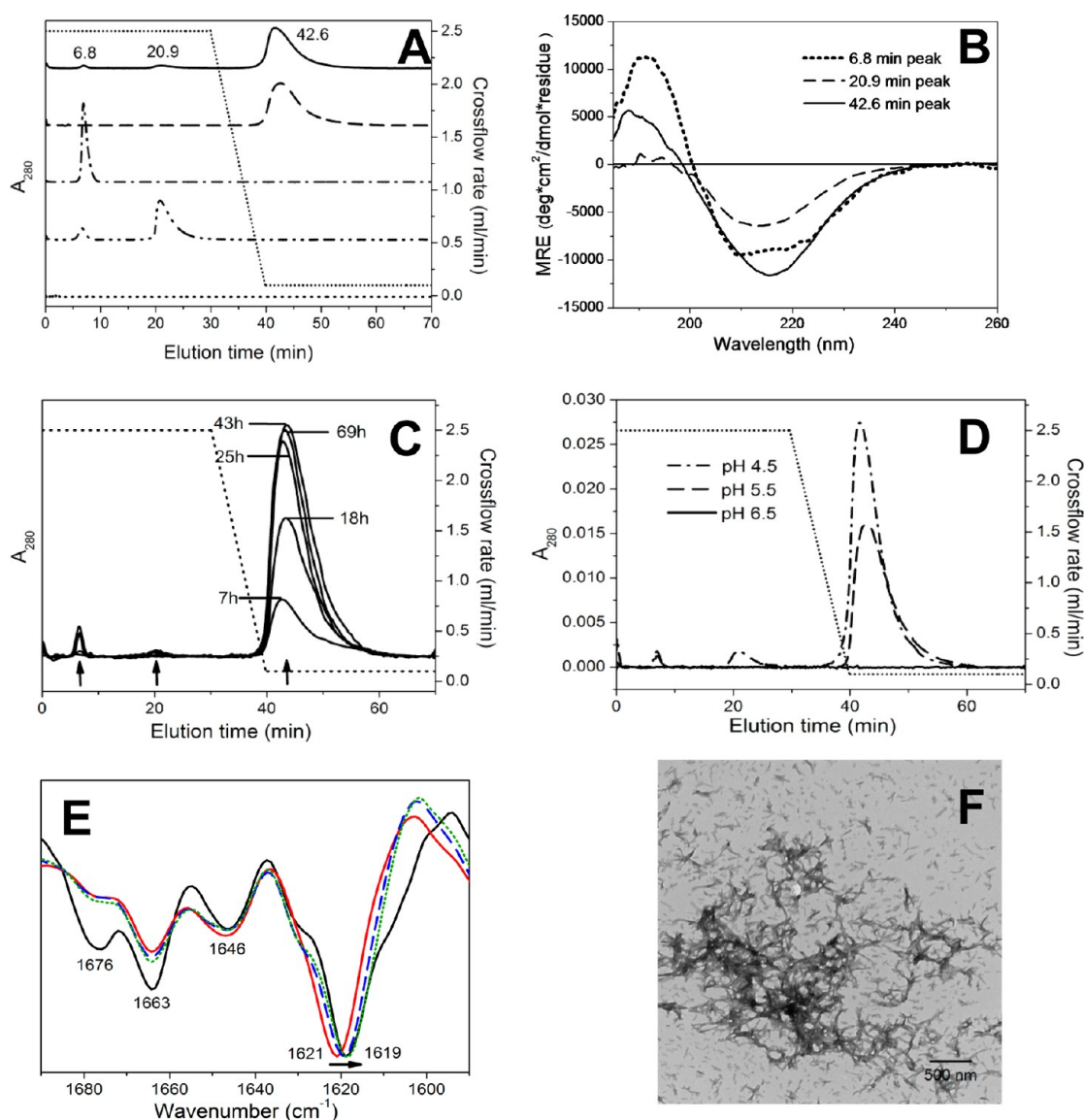


**Figure 3.** Biophysical characterization of rPrP23–232 protofilaments. (A) AF4 analysis of rPrP23–232 conformers: the low-pH supernatant (—), re-injection of the 42.6 min protofilament peak 72 h after collection (— · —), pure  $\alpha$ -monomer (— · —), and pure  $\beta$ -oligomer (— · —). The elution profile of low-pH-treated rPrP90–232 fibrils (·· ·) is included for comparison. (B) CD spectra of the supernatant components after separation by AF4. (C) Time course of protofilament formation as monitored by AF4. (D) pH dependence of protofilament formation. (E) Second-derivative FT-IR spectra of protofilaments at pH 4.5 (red) and 10 min (blue) and 72 h (green) after the pH had been increased to 7.0. The spectrum of the parent fibrils at pH 7.0 is included for comparison (black). (F) TEM image of aggregates formed after 72 h at pH 7.0.

**Table 1. Secondary Structure Composition of rPrP23–232 Conformers**

secondary structure type	$\alpha$ -monomer	$\beta$ -oligomer	protofilaments
$\alpha$ -helix	23%	4%	7%
$\beta$ -sheet	26%	38%	30%
turn	21%	25%	25%
loop/unordered	29%	32%	37%

published;<sup>56</sup> however, these fibrils were in an acidic buffer, and thus, the reported CD signal may actually be that of dissociated, soluble protofilaments.

**FT-IR Spectroscopy.** We compared the secondary structure of the soluble protofilaments with that of their parent rPrP23–232 fibrils using FT-IR spectroscopy (Figure 3E). Unlike CD, FT-IR spectroscopy may be used for both solution and solid samples and is better suited for the characterization of  $\beta$ -sheet

structure. When the limitations of both techniques are taken into account, the FT-IR results are reasonably consistent with the results obtained from CD. The high cross- $\beta$ -sheet content of protofilaments is evident in the strong single amide I band centered at  $1621\text{ cm}^{-1}$  (solid red line), which is shifted to slightly higher frequency as compared with the recombinant fibrils ( $1619\text{ cm}^{-1}$ , solid black line). A shoulder at  $1628\text{ cm}^{-1}$  in the fibril spectrum is absent in the protofilament spectrum. The amide I bands previously assigned to turns and loops ( $1663$  and  $1676\text{ cm}^{-1}$ , respectively)<sup>32,56,57</sup> were less substantial in protofilaments than in fibrils, possibly indicating some unfolding of these structures. Overall, the spectrum of protofilaments is quite similar to that of the parent fibrils.

Increasing the pH of the protofilaments to 7.0 caused an immediate shift of the  $\beta$ -sheet amide I band from  $1621$  to  $1619\text{ cm}^{-1}$ , and the shoulder at  $1628\text{ cm}^{-1}$  appeared, becoming more defined after incubation for 72 h at pH 7.0 (Figure 3E, dashed

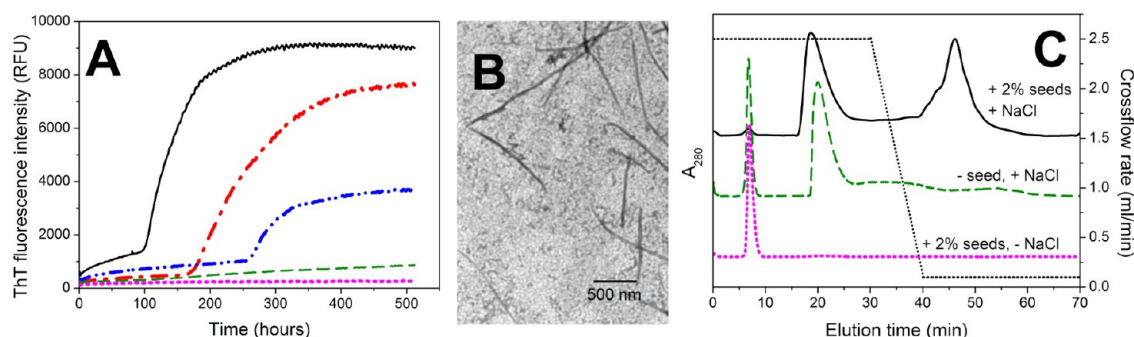


**Figure 4.** Protofilament-seeded conversion of rPrP23–232  $\alpha$ -monomer under mildly acidic, nondenaturing conditions. (A) Kinetics as followed by a ThT fluorescence assay. Seed concentrations were 2% (black), 1% (red), 0.5% (blue), and 0% (green), and  $\alpha$ -monomer with 2% seed in the absence of NaCl (magenta). (B) TEM image of products of a 2% seeded reaction with NaCl formed after 3 weeks. (C) AF4 analysis of the conversion products of 2% seed with NaCl (black), 0% seed with NaCl (green), and 2% seed without NaCl (magenta).

blue and dotted green lines). Overall, the data suggest that the minor differences in the  $\beta$ -strand structure between protofilaments at acidic pH and fibrils are pH-dependent and largely reversible. However, we did not observe any reassembly of protofilaments into twisted or parallel fibrils by TEM; instead, clumps of aggregates were formed when the pH was increased (Figure 3F). In regions of the TEM image where individual structures could be isolated and measured, the widths of the structures were  $\sim 14$  nm, resembling protofilaments and not fibrils.

Overall, the biophysical and spectroscopic data suggest the main structural characteristics of amyloid fibrils are preserved in the soluble protofilaments.

**Ability of Protofilaments To Accelerate Conversion of  $\alpha$ -Monomeric PrP.** Typical fibril formation shows a characteristic nucleation-dependent pattern with three kinetic phases: the initial lag phase is followed by a steep log phase and then a final plateau. It has been well-established that in the presence of preformed fibril seeds, conversion under partially denaturing conditions is accelerated with a dramatically shortened lag phase.<sup>32</sup> We examined whether this also held true for preformed protofilament seeds under physiologically relevant conditions, i.e., in the absence of denaturants.

Propagation experiments were performed using conformers of rPrP23–232 in 20 mM acetate and 0.1 M NaCl (pH 4.5) to approximate the environment of late endosomal vesicles. A direct comparison between fibrils and protofilaments was not possible because fibrils dissociate into protofilaments of varying lengths in less than 24 h at pH 4.5. Similarly, protofilaments form amorphous aggregates at neutral pH.

The ratio of soluble protofilaments (seeds) to  $\alpha$ -monomer was varied from 0 to 2% (Figure 4A). The unseeded control samples showed little change even after 3 weeks, but all seeded experiments followed a typical nucleation-dependent polymerization mechanism. Adding more protofilament seeds proportionally shortened the incubation times and increased both the rate of the log phase kinetics and the final plateau levels of ThT fluorescence intensity. However, overall the lag phase was significantly elongated (days) as compared with reactions conducted in the presence of denaturants (hours).<sup>32</sup>

After 3 weeks, the products from the 2% seeded reaction were examined by TEM imaging (Figure 4B). There were considerable amounts of small particles present in the sample. This was confirmed by AF4 (Figure 4C, top trace), which detected both  $\beta$ -oligomer (retention time of 20.9 min) and ThT-binding high-molecular mass aggregates that were larger

than the seeds themselves (broad peak with a retention time of  $\sim 46$  min). Control experiments showed that this peak results from conversion of the  $\alpha$ -monomer, as the seeds themselves (retention time of 42.6 min) are undetectable at the highest concentration used (bottom trace).

The TEM image in Figure 4B also indicated that some highly elongated, unbranched structures had also formed in the reaction, with an approximate width of  $34 \pm 5$  nm. This width matches that of the parent fibrils produced under partially denaturing conditions (Figure 1E) and not that of the protofilament seeds.

Consistent with previous reports,<sup>58</sup>  $\alpha$ -monomers are quite stable in the absence of salt, even when 2% seeds are added (Figure 4C, magenta). The destabilizing effect of salt is notable in the unseeded control (green), where the magnitude of the peak at 6.8 min has decreased and larger products appear at longer retention times. The major product is the  $\beta$ -oligomer (peak at 20.9 min). Small amounts of non-ThT-binding aggregates are also formed, which result in the elevated baseline at later elution times.

## DISCUSSION

**Mechanism of Dissociation of Fibrils into Protofilaments.** This study demonstrates that full-length rPrP fibrils dissociate when they are exposed to mildly acidic conditions. As judged from microscopy imaging (Figure 1), dissociation occurs in two dimensions, lateral and axial. Lateral dissociation involves the disassembly of mature fibrils into constituent protofilaments, while axial dissociation further divides the protofilaments along the fibrillar axis into smaller entities of variable lengths. To the best of our knowledge, the ability of mature amyloid fibrils to undergo dissociation into protofilaments under mildly acidic conditions has not been previously reported. The pH conditions used here are similar to those found in late endosomal and lysosomal vesicles. Kinetic analysis shows that the protofilaments preserve the ability to propagate in vitro (Figure 4) and thus may be physiologically relevant, as our conditions mimic those of late endocytic and lysosomal vesicles.

Fibril dissociation is necessary for efficient propagation of the prion state. Two possible mechanisms for fibril dissociation have been proposed in the literature: mechanical stress-induced dissociation and chaperone-mediated dissociation.<sup>21,59</sup> The results from this study suggest another possible mechanism, dissociation of fibrils into protofilaments induced by low pH. The lack of dissociation in N-terminally truncated fibrils



(rPrP90–232) at low pH indicates that the N-terminal region of PrP is important to the dissociation process. In full-length hamster PrP, this region (residues 23–140) is quite basic, containing no Asp, no Glu, four Arg, seven Lys, and seven His residues; this pattern is highly conserved among mammalian PrPs. His residues have a  $pK_a$  of  $\sim 6.8$  and thus are the only residues present that could account for the observed pH effect. We hypothesize that protonation of His residues in a domain already enriched with positively charged residues leads to charge repulsion, which causes the dissociation of fibrillar superstructures into protofilaments. Conformational perturbations induced by charge repulsion in residues 90–140 (contains three of the conserved His residues) have been reported in studies of human truncated rPrP90–231, with an associated  $pK_a$  of 5.3.<sup>60</sup> Given that we did not observe dissociation of N-terminally truncated fibrils (hamster rPrP90–232) into protofilaments, we postulate that the four additional His residues found in the stretch of residues 23–89 play an important role in acid-induced fibril dissociation. Additional studies to test this hypothesis are underway.

**Protofilament Structure and Seeding Capability.** Some of the protofilaments were sufficiently small to be considered soluble (Figures 1 and 2). These have an average length of  $\sim 65$  nm and an apparent molecular mass of  $\sim 5.8$  MDa ( $\sim 250$  monomeric subunits). The soluble protofilaments retain the hallmark characteristics of full-length amyloid fibrils and share the same amyloid core. Small but largely reversible pH-dependent differences in the  $\beta$ -sheet core structure were noted by FT-IR. The protofilaments have a unique CD spectrum compared with those of other soluble forms of PrP.

At pH 4.5 in the presence of 0.1 M NaCl and  $\alpha$ -monomer, protofilaments are efficient seeds (Figure 4). The propagated products are mostly elongated protofilaments, though a few fibrils can be detected after several weeks. This fits with our initial observations that the yield of soluble protofilaments from parent fibrils was higher when salt was omitted from the acidic buffer. It is likely that the presence of counterions in the buffer shields the large positive charge on the N-terminal domains of individual protofilaments, permitting some fibrils to be formed when there is an excess of  $\alpha$ -monomer present. As previously reported, destabilization of the  $\alpha$ -monomer in the presence of NaCl also facilitates the conversion process.<sup>58</sup>

**Physiologic Relevance of pH-Induced Protofilament Formation.** A number of studies have proposed that the endocytic pathway, including endosomes and lysosomes, is important for PrP<sup>Sc</sup> conversion in vivo.<sup>14,20–23</sup> Although most efforts have been devoted to illustrating the destabilizing effect of these acidic vesicles on the global structure and thermodynamic stability of PrP<sup>C</sup>,<sup>61–63</sup> less attention has been paid to its impact on mature amyloids. We show here that in addition to destabilizing  $\alpha$ -monomers and thus facilitating primary nucleation, low pH may also contribute to fibril dissociation, a secondary nucleation event that is necessary for efficient conversion and maintenance of the prion state.<sup>64</sup> Results of these in vitro studies offer direct evidence that at low pH, mature fibrils can dissociate both laterally and axially into protofilaments, which are then able to recruit and convert  $\alpha$ -monomer. Assuming that a similar dissociation mechanism is used in vivo, protofilaments of PrP<sup>Sc</sup> formed in the lysosome might be excellent seeds for the propagation of PrP<sup>C</sup> during its normal recycling from the cell surface via the endocytic pathway.<sup>20</sup>

In summary, we provide experimental evidence that mildly acidic conditions resembling those of late endosomal and lysosomal vesicles are sufficient to dissociate rPrP23–232 fibrils laterally and axially. The dissociation is believed to involve charge repulsion of protonated His residues in the N-terminal domain. The protofilaments thus formed retain amyloid characteristics and are competent seeds for propagating new prions. Thus, late endocytic and lysosomal vesicles are sites of efficient prion propagation not only because they destabilize the  $\alpha$ -monomer but also because they accelerate the dissociation of fibrils into protofilament seeds.

## ■ ASSOCIATED CONTENT

### ● Supporting Information

Thermal denaturation and ThT fluorescence of soluble protofilaments, mass spectrometry data that identify their amyloid core, and MALS determination of molar masses. This material is available free of charge via the Internet at <http://pubs.acs.org>.

## ■ AUTHOR INFORMATION

### Corresponding Author

\*Division of Biological Sciences, 204 CHCB, The University of Montana, Missoula, MT 59812. E-mail: [michele.mcguirl@umontana.edu](mailto:michele.mcguirl@umontana.edu). Telephone: (406) 243-4404. Fax: (406) 243-4304.

### Funding

This work was supported by National Institutes of Health (NIH) Grant 1R01-GM081649 (M.A.M.), Office of Naval Research IDEA Grant DAMD-17-03-1-0342 (M.A.M.), and a subproject award (M.A.M.) from NIH COBRE Grant SP20-RR020185-03 (A. Harmson, Principal Investigator). Images, electron microscopy services, and resources were provided by the Electron Microscopy Facility at The University of Montana, which is supported by the National Center for Research Resources (SP20RR016455-11) and the National Institute of General Medical Sciences (8 P20 GM103474-11).

### Notes

The authors declare no competing financial interest.

## ■ ACKNOWLEDGMENTS

We thank the Montana State University Mass Spectrometry Core Facility and Jonathan Hilmer, Brian Bothner, and Jared Bowden for assistance collecting MALDI-ToF/ToF data and Lara Taubner for many helpful discussions. We also thank Jim Driver at the University of Montana Electron Microscopy Facility for assistance collecting TEM images.

## ■ ABBREVIATIONS

AF4, asymmetric flow field flow fractionation; CD, circular dichroism; MRE, mean residue ellipticity; PK, proteinase K; PrP, hamster prion protein; PrP<sup>C</sup>, normal cellular PrP; PrP<sup>Sc</sup>, infectious misfolded PrP; rPrP23–232, full-length recombinant PrP; rPrP90–232, N-terminally truncated recombinant PrP; TEM, transmission electron microscopy; ThT, thioflavin T.

## ■ REFERENCES

- (1) Stahl, N., Borchelt, D. R., Hsiao, K., and Prusiner, S. B. (1987) Scrapie prion protein contains a phosphatidylinositol glycolipid. *Cell* 51, 229–240.

- (2) Kim, Y., Lee, J., and Lee, C. (2008) In silico comparative analysis of DNA and amino acid sequences for prion protein gene. *Transbound. Emerging Dis.* 55, 105–114.
- (3) Herms, J., Tings, T., Gall, S., Madlung, A., Giese, A., Siebert, H., Schurmann, P., Windl, O., Brose, N., and Kretzschmar, H. (1999) Evidence of presynaptic location and function of the prion protein. *J. Neurosci.* 19, 8866–8875.
- (4) Riek, R., Hornemann, S., Wider, G., Billeter, M., Glockshuber, R., and Wuthrich, K. (1996) NMR structure of the mouse prion protein domain PrP(121–321). *Nature* 382, 180–182.
- (5) Knaus, K. J., Morillas, M., Swietnicki, W., Malone, M., Surewicz, W. K., and Yee, V. C. (2001) Crystal structure of the human prion protein reveals a mechanism for oligomerization. *Nat. Struct. Biol.* 8, 770–774.
- (6) Wuthrich, K., and Riek, R. (2001) Three-dimensional structures of prion proteins. *Adv. Protein Chem.* 57, 55–82.
- (7) Moore, R. A., Taubner, L. M., and Priola, S. A. (2009) Prion protein misfolding and disease. *Curr. Opin. Struct. Biol.* 19, 14–22.
- (8) Prusiner, S. B. (1998) Prions. *Proc. Natl. Acad. Sci. U.S.A.* 95, 13363–13383.
- (9) Prusiner, S. B. (1982) Novel proteinaceous infectious particles cause scrapie. *Science* 216, 136–144.
- (10) Radford, H. E., and Mallucci, G. R. (2009) The Role of GPI-anchored PrP(C) in Mediating the Neurotoxic Effect of Scrapie Prions in Neurons. *Curr. Issues Mol. Biol.* 12, 119–128.
- (11) Mallucci, G. R., White, M. D., Farmer, M., Dickinson, A., Khatun, H., Powell, A. D., Brandner, S., Jefferys, J. G., and Collinge, J. (2007) Targeting cellular prion protein reverses early cognitive deficits and neurophysiological dysfunction in prion-infected mice. *Neuron* 53, 325–335.
- (12) Soto, C. (2007) Reversibility of prion-induced neurodegeneration. *Lancet Neurol.* 6, 294–295.
- (13) Collinge, J., and Clarke, A. R. (2007) A general model of prion strains and their pathogenicity. *Science* 318, 930–936.
- (14) Caughey, B., and Baron, G. S. (2006) Prions and their partners in crime. *Nature* 443, 803–810.
- (15) Cobb, N. J., and Surewicz, W. K. (2009) Prion diseases and their biochemical mechanisms. *Biochemistry* 48, 2574–2585.
- (16) Padrick, S. B., and Miranker, A. D. (2002) Islet amyloid: Phase partitioning and secondary nucleation are central to the mechanism of fibrillogenesis. *Biochemistry* 41, 4694–4703.
- (17) Wall, J., Schell, M., Murphy, C., Hrnčić, R., Stevens, F. J., and Solomon, A. (1999) Thermodynamic instability of human lambda 6 light chains: Correlation with fibrillogenicity. *Biochemistry* 38, 14101–14108.
- (18) Zampieri, M., Legname, G., and Altafini, C. (2009) Investigating the conformational stability of prion strains through a kinetic replication model. *PLoS Comput. Biol.* 5, e1000420.
- (19) Knowles, T. P., Waudby, C. A., Devlin, G. L., Cohen, S. I., Aguzzi, A., Vendruscolo, M., Terentjev, E. M., Welland, M. E., and Dobson, C. M. (2009) An analytical solution to the kinetics of breakable filament assembly. *Science* 326, 1533–1537.
- (20) Caughey, B., Baron, G. S., Chesebro, B., and Jeffrey, M. (2009) Getting a grip on prions: Oligomers, amyloids, and pathological membrane interactions. *Annu. Rev. Biochem.* 78, 177–204.
- (21) Lee, K. S., and Caughey, B. (2007) A simplified recipe for prions. *Proc. Natl. Acad. Sci. U.S.A.* 104, 9551–9552.
- (22) Marijanovic, Z., Caputo, A., Campana, V., and Zurzolo, C. (2009) Identification of an intracellular site of prion conversion. *PLoS Pathog.* 5, e1000426.
- (23) Borchelt, D. R., Taraboulos, A., and Prusiner, S. B. (1992) Evidence for synthesis of scrapie prion proteins in the endocytic pathway. *J. Biol. Chem.* 267, 16188–16199.
- (24) Taraboulos, A., Serban, D., and Prusiner, S. B. (1990) Scrapie prion proteins accumulate in the cytoplasm of persistently infected cultured cells. *J. Cell Biol.* 110, 2117–2132.
- (25) Heiseke, A., Agui, Y., and Schatzl, H. M. (2010) Autophagy, prion infection and their mutual interactions. *Curr. Issues Mol. Biol.* 12, 87–97.
- (26) Lee, R. J., Wang, S., and Low, P. S. (1996) Measurement of endosome pH following folate receptor-mediated endocytosis. *Biochim. Biophys. Acta* 1312, 237–242.
- (27) Speare, J. O., Rush, T. S., III, Bloom, M. E., and Caughey, B. (2003) The role of helix 1 aspartates and salt bridges in the stability and conversion of prion protein. *J. Biol. Chem.* 278, 12522–12529.
- (28) Lennon, C. W., Cox, H. D., Hennelly, S. P., Chelmo, S. J., and McGuire, M. A. (2007) Probing structural differences in prion protein isoforms by tyrosine nitration. *Biochemistry* 46, 4850–4860.
- (29) Gasteiger, E., Hoogland, C., Gattiker, A., Duvaud, S., Wilkins, M. R., Appel, R. D., and Bairoch, A. (2005) Protein Identification and Analysis Tools on the ExPASy Server. In *The Proteomics Protocols Handbook* (Walker, J. M., Ed.) pp 571–607, Humana Press, Totowa, NJ.
- (30) DeMarco, M. L., and Daggett, V. (2009) Characterization of cell-surface prion protein relative to its recombinant analogue: Insights from molecular dynamics simulations of diglycosylated, membrane-bound human prion protein. *J. Neurochem.* 109, 60–73.
- (31) Baskakov, I. V., Legname, G., Prusiner, S. B., and Cohen, F. E. (2001) Folding of prion protein to its native  $\alpha$ -helical conformation is under kinetic control. *J. Biol. Chem.* 276, 19687–19690.
- (32) Bocharova, O. V., Breydo, L., Parfenov, A. S., Salnikov, V. V., and Baskakov, I. V. (2005) In vitro conversion of full-length mammalian prion protein produces amyloid form with physical properties of PrP(Sc). *J. Mol. Biol.* 346, 645–659.
- (33) Tahiri-Alaoui, A., and James, W. (2005) Rapid formation of amyloid from  $\alpha$ -monomeric recombinant human PrP in vitro. *Protein Sci.* 14, 942–947.
- (34) Atarashi, R., Moore, R. A., Sim, V. L., Hughson, A. G., Dorward, D. W., Onwubiko, H. A., Priola, S. A., and Caughey, B. (2007) Ultrasensitive detection of scrapie prion protein using seeded conversion of recombinant prion protein. *Nat. Methods* 4, 645–650.
- (35) Baskakov, I. V., Legname, G., Baldwin, M. A., Prusiner, S. B., and Cohen, F. E. (2002) Pathway complexity of prion protein assembly into amyloid. *J. Biol. Chem.* 277, 21140–21148.
- (36) Silveira, J. R., Hughson, A. G., and Caughey, B. (2006) Fractionation of prion protein aggregates by asymmetrical flow field-flow fractionation. *Methods Enzymol.* 412, 21–33.
- (37) Moon, M. H., Williams, P. S., Kang, D., and Hwang, I. (2002) Field and flow programming in frit-inlet asymmetrical flow field-flow fractionation. *J. Chromatogr., A* 955, 263–272.
- (38) Giddings, J. C., and Caldwell, K. D. (1984) Field-flow fractionation: Choices in programmed and nonprogrammed operation. *Anal. Chem.* 56, 2093–2099.
- (39) Wyatt, P. J. (1993) Light scattering and the absolute characterization of macromolecules. *Anal. Chim. Acta* 272, 1–40.
- (40) Andersson, M., Wittgren, B., and Wahlund, K. G. (2003) Accuracy in multiangle light scattering measurements for molar mass and radius estimations. Model calculations and experiments. *Anal. Chem.* 75, 4279–4291.
- (41) Lee, S., Nilsson, P. O., Nilsson, G. S., and Wahlund, K. G. (2003) Development of asymmetrical flow field-flow fractionation-multi angle laser light scattering analysis for molecular mass characterization of cationic potato amylopectin. *J. Chromatogr., A* 1011, 111–123.
- (42) Halliday, D., and Resnick, R. (1960) in *Physics for Students of Science and Engineering, Combined Edition*, pp 216–244, John Wiley & Sons Inc., New York.
- (43) Pelton, J. T., and McLean, L. R. (2000) Spectroscopic methods for analysis of protein secondary structure. *Anal. Biochem.* 277, 167–176.
- (44) Lohley, A., Whitmore, L., and Wallace, B. A. (2002) DICHROWEB: An interactive website for the analysis of protein secondary structure from circular dichroism spectra. *Bioinformatics* 18, 211–212.
- (45) Whitmore, L., and Wallace, B. A. (2004) DICHROWEB, an online server for protein secondary structure analyses from circular dichroism spectroscopic data. *Nucleic Acids Res.* 32, W668–W673.



- (46) Surewicz, W. K., Mantsch, H. H., and Chapman, D. (1993) Determination of protein secondary structure by Fourier transform infrared spectroscopy: A critical assessment. *Biochemistry* 32, 389–394.
- (47) Dong, A., Huang, P., and Caughey, W. S. (1990) Protein secondary structures in water from second-derivative amide I infrared spectra. *Biochemistry* 29, 3303–3308.
- (48) Shevchenko, A., Wilm, M., Vorm, O., and Mann, M. (1996) Mass spectrometric sequencing of proteins silver-stained polyacrylamide gels. *Anal. Chem.* 68, 850–858.
- (49) Strohal, M., Kavan, D., Novak, P., Volny, M., and Havlicek, V. (2010) mMass 3: A cross-platform software environment for precise analysis of mass spectrometric data. *Anal. Chem.* 82, 4648–4651.
- (50) Bocharova, O. V., Breydo, L., Salnikov, V. V., and Baskakov, I. V. (2005) Copper(II) inhibits in vitro conversion of prion protein into amyloid fibrils. *Biochemistry* 44, 6776–6787.
- (51) Sim, V. L., and Caughey, B. (2009) Ultrastructures and strain comparison of under-glycosylated scrapie prion fibrils. *Neurobiol. Aging* 30, 2031–2042.
- (52) Hjelmeland, L. M., and Chrambach, A. (1984) Solubilization of functional membrane proteins. *Methods Enzymol.* 104, 305–318.
- (53) Notari, S., Capellari, S., Giese, A., Westner, I., Baruzzi, A., Ghetti, B., Gambetti, P., Kretzschmar, H. A., and Parchi, P. (2004) Effects of different experimental conditions on the PrP<sup>Sc</sup> core generated by protease digestion: Implications for strain typing and molecular classification of CJD. *J. Biol. Chem.* 279, 16797–16804.
- (54) Lu, X., Wintrod, P. L., and Surewicz, W. K. (2007)  $\beta$ -Sheet core of human prion protein amyloid fibrils as determined by hydrogen/deuterium exchange. *Proc. Natl. Acad. Sci. U.S.A.* 104, 1510–1515.
- (55) Cobb, N. J., Sonnichsen, F. D., McHaourab, H., and Surewicz, W. K. (2007) Molecular architecture of human prion protein amyloid: A parallel, in-register  $\beta$ -structure. *Proc. Natl. Acad. Sci. U.S.A.* 104, 18946–18951.
- (56) Ostapchenko, V. G., Sawaya, M. R., Makarava, N., Savtchenko, R., Nilsson, K. P., Eisenberg, D., and Baskakov, I. V. (2010) Two amyloid states of the prion protein display significantly different folding patterns. *J. Mol. Biol.* 400, 908–921.
- (57) Ollesch, J., Kunemann, E., Glockshuber, R., and Gerwert, K. (2007) Prion protein  $\alpha$ -to- $\beta$  transition monitored by time-resolved Fourier transform infrared spectroscopy. *Appl. Spectrosc.* 61, 1025–1031.
- (58) Apetri, A. C., and Surewicz, W. K. (2003) Atypical effect of salts on the thermodynamic stability of human prion protein. *J. Biol. Chem.* 278, 22187–22192.
- (59) Sun, Y., Makarava, N., Lee, C. I., Laksanalamai, P., Robb, F. T., and Baskakov, I. V. (2008) Conformational stability of PrP amyloid fibrils controls their smallest possible fragment size. *J. Mol. Biol.* 376, 1155–1167.
- (60) Cobb, N. J., Apetri, A. C., and Surewicz, W. K. (2008) Prion protein amyloid formation under native-like conditions involves refolding of the C-terminal  $\alpha$ -helical domain. *J. Biol. Chem.* 283, 34704–34711.
- (61) Kelly, J. W. (1998) The alternative conformations of amyloidogenic proteins and their multi-step assembly pathways. *Curr. Opin. Struct. Biol.* 8, 101–106.
- (62) van der Kamp, M. W., and Daggett, V. (2010) Influence of pH on the human prion protein: Insights into the early steps of misfolding. *Biophys. J.* 99, 2289–2298.
- (63) Campos, S. R., Machuqueiro, M., and Baptista, A. M. (2010) Constant-pH molecular dynamics simulations reveal a  $\beta$ -rich form of the human prion protein. *J. Phys. Chem. B* 114, 12692–12700.
- (64) Wang, Y. Q., Buell, A. K., Wang, X. Y., Welland, M. E., Dobson, C. M., Knowles, T. P., and Perrett, S. (2011) Relationship between Prion Propensity and the Rates of Individual Molecular Steps of Fibril Assembly. *J. Biol. Chem.* 286, 12101–12107.